Self-pinching of a relativistic electron bunch in a drift tube

Claudio G. Parazzoli and Benjamin E.C. Koltenbah

The Boeing Company, Boeing Defense & Space Group, P.O. Box 3999, M/S 87-85 Seattle, WA 98124-2499, USA

Abstract

Electron bunches with charge densities ρ of the order of 10^2 to 10^3 [nC/cm^3], energies between 20. and 100. [MeV], peak current > 100 [A], bunch lengths between 0.3 and 1.8 [cm], and bunch charge of 2.0 to 20. [nC] are relevant to the design of Free Electron Lasers and future linear colliders. In this paper we present the results of numerical simulations performed with a particle in a cell (pic) code of an electron bunch in a drift tube. The electron bunch has cylindrical symmetry with the z-axis oriented in the direction of motion. The charge density distribution is constant in the radial and Gaussian in the longitudinal direction, respectively. The electron bunch experiences both a radial pinch in the middle of the pulse, corresponding to the peak electron density, and a significant growth of the correlated emittance. This behavior is explained, and an approximate scaling law is identified. Comparisons of the results from the pic and PARMELA codes are presented.

1 Introduction

New designs of Free Electron Lasers and high-brightness colliders require the modeling of electron bunches with higher charge densities than have previously been studied. In this high-charge regime, self-fields must be handled consistently. "Particle-in-a-cell", or pic, codes must therefore be employed instead of the commonly-used "particle-pusher" codes, such as PARMELA, which do not account completely for self-fields. We studied the simple case of a bunch traveling along a drift tube in order to gain a better understanding of the self-field effects in this high-charge regime. We have completed a detailed series of calculations using a pic code (detailed below) on a range of energy and electron charge where significant disagreement between pic and "particle-pusher" codes has been found. Our results display rather severe self-pinching of the bunch under certain circumstances, implying the existence of a radially inward-directed force which we explain analytically.

The outline of the paper is as follows: Section 2 contains a discussion of the forces acting on an electron bunch, the origin of the radial pinching, and an estimate of the initial space charge potential. Section 3 contains numerical results of the pic code, a discussion of the scaling parameters, and comparison between the pic and PARMELA codes results. Section 4 contains a summary of the paper and conclusions.

2 Radial pinching force and space charge potential

It is well known [1,2] that for an infinitely long relativistic electron beam, traveling in the positive z-direction and having constant electron density along z, the outward-directed radial space charge force is nearly balanced by the inward-directed Lorentz force. The electron beam is thus subjected to a small net defocusing effect. In this section we show, for the case of a finite length electron bunch, the origin of a radial force which is directed inward and which generates a pinch in the electron bunch envelope as seen in Figure 1. The motion of the particles is in the positive z-direction, cylindrical symmetry is assumed, and the relative longitudinal particle position in the bunch is denoted by ζ, where $\zeta = z - z_c$, and z_c is the z-position of the center of the bunch.
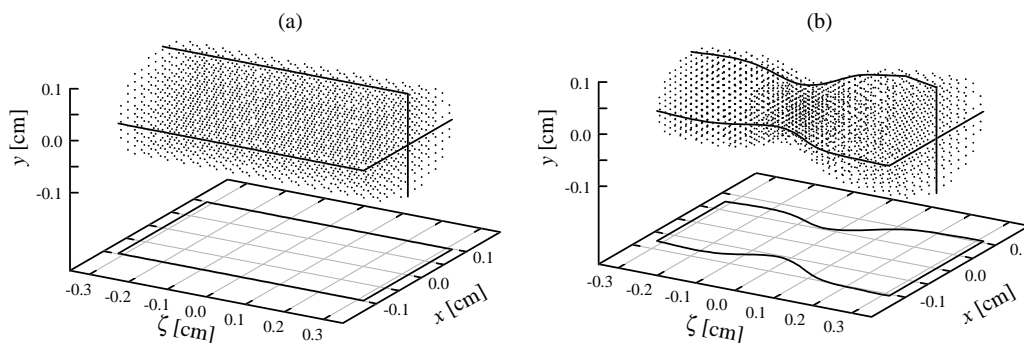

Fig. 1. Electron bunch and bunch envelope at drift positions (a) $z_c = 0$ [cm] (drift entrance) and (b) $z_c = 30.$ [cm] (drift exit). The pulse envelope is projected on the bottom panel. Bunch parameters: $Q = 2.0$ [nC], $a = 0.1$ [cm], $\sigma = 0.1274$ [cm], $b = 1.5$ [cm], $E = 20.0$ [MeV], $\gamma_0 = 40.138$.

We assume, following [3], that all the electrons travel along z with uniform velocity $v = \beta_0 c$, no transverse velocity component is present, and the density $\rho(r, z)$ is given by

$$\rho(r, s(z,t)) = \begin{cases} Q/(\pi a^2)\ f(s) = n_o f(s) & : \quad r < a \\ 0 & : \quad r > a, \end{cases} \tag{1}$$

where $s = z - \beta_0 ct$, $f(s) = \mathrm{e}^{-(s/\sigma)^2/2}\,/[(2\pi)^{1/2}\sigma]$ is the normalized longitudinal

density distribution, Q is the pulse charge with appropriate sign, and a is the electron bunch radius. We further assume that the z- and t-dependencies of the electric field E and magnetic field B in Maxwell's equations are combined in the variable s. This *ansatz* is appropriate when the electrons have a common longitudinal velocity β_0 and no transverse motion. This assumption is violated, as shown by the numerical simulations, after the bunch drifts a significant distance. It is, however, useful to establish the conditions for the onset of the radial pinching force. The region in which we will solve Maxwell's equations is the inside of a perfectly conductive drift tube of radius b.

In view of the symmetry of the problem, only the E_r^0, E_x^0, and B_θ^0 components of the fields are present. The superscript $()^0$ is used to indicate that the fields are computed in the absence of any transverse velocity.

The Fourier transform of the electric field is

$$\vec{\mathcal{E}}(k, r) = (2\pi)^{-1} \int \vec{E}(r, s) \, e^{-iks} \, ds, \tag{2}$$

and similar definitions hold for the Fourier transforms $\vec{\mathcal{B}}(k, r)$ and $\mathcal{F}(k)$ of $\vec{B}(r, s)$ and $f(s)$, respectively. For our selection of $f(s)$, a Gaussian distribution with standard deviation σ is assumed, and $\mathcal{F}(k) = e^{-(k\sigma)^2/2}$.

Upon substitution into Maxwell's equations, $\mathcal{E}_r^0$ and $\mathcal{B}_\theta^0$ can be expressed as functions of $\mathcal{E}_z^0$ only, and inside the perfectly conductive drift tube the results are as follows:

$$\mathcal{E}_r^0 = \frac{ik}{q^2} \frac{\partial \mathcal{E}_z^0}{\partial r}, \tag{3}$$

$$\mathcal{B}_\theta^0 = \frac{ikb}{q^2} \frac{\partial \mathcal{E}_z^0}{\partial r}, \tag{4}$$

where $q = -ik/\gamma_0$ and $\gamma_0^2 = (1 - \beta_0^2)^{-1}$. In the region inside the electron bunch, where $r < a$, the differential equation satisfied by $\mathcal{E}_z^0$ is

$$\frac{1}{r} \frac{\partial}{\partial r} \left(r \frac{\partial \mathcal{E}_z^0}{\partial r} \right) + q^2 \mathcal{E}_z^0 = i \frac{4\pi n_0}{\gamma_0^2} k \mathcal{F}(k), \tag{5}$$

and in the region outside the electron bunch, where $a < r < b$,

$$\frac{1}{r} \frac{\partial}{\partial r} \left(r \frac{\partial \mathcal{E}_z^0}{\partial r} \right) + q^2 \mathcal{E}_z^0 = 0. \tag{6}$$

The solution of Eqs. (5) and (6) must be finite, continuos everywhere, vanish

at the conductive wall of the drift tube ($r = b$) and insure the continuity of $\mathcal{E}_r^0$ at the edge of the pulse ($r = a$). The solution is

$$
\mathcal{E}_z^0(k,r) = \begin{cases} C_1 J_0(qr) + 4\pi n_0 \; \mathcal{F}(k)/(\mathrm{i}k) & : \quad r < a \\[2mm] [C_1 - 2\pi^2 n_0 qa Y_1(qa) \; \mathcal{F}(k)/(\mathrm{i}k)] \; J_0(qr) \\[2mm] +[2\pi^2 n_0 qa J_1(qa) \; \mathcal{F}(k)/(\mathrm{i}k)] \; Y_0(qr) \end{cases} \quad : \quad r > a,
\tag{7}
$$

where J_n and Y_n are the Bessel functions of first and second kind [4]. The integration constant C_1 is

$$
C_1 = 2\pi^2 n_0 qa \; \chi(q) \; \mathcal{F}(k)/(\mathrm{i}k), \quad \text{where}
\tag{8}
$$
$$
\chi(q) = [Y_1(qa) \; J_0(qb) - J_1(qa) \; Y_0(qb)] \; / \; J_0(qb).
\tag{9}
$$

2.1 Calculation of the radial force

The zeroth order calculation of the radial force, F_s^0, neglects the electron radial motion induced by the space charge and Lorentz force, i.e. the electron bunch moves as a solid body. F_s^0 is the sum of the radial space charge force and the Lorentz force arising from the poloidal magnetic field B_θ^0 and the longitudinal velocity of the electrons:

$$
F_s^0 = e(E_r^0 - \beta B_\theta^0),
\tag{10}
$$

where e is the electronic charge with appropriate sign. With the help of Eqs. (3), (4), and (7) (for $r < a$), we find for the radial force

$$
F_s^0 = -(1 - \beta_0^2)\frac{Qe}{a} \int\limits_{-\infty}^{\infty} \mathrm{d}k \, \mathrm{e}^{\mathrm{i}ks-(k\sigma)^2/2} \chi(\mathrm{i}k/\gamma_0) J_1(\mathrm{i}kr/\gamma_0)
$$
$$
= (1 - \beta_0^2) E_r^0.
\tag{11}
$$

It is simple to verify that the integral is always real and negative, thus the radial force is directed outward and corresponds to a defocusing of the electron pulse. This result is a simple generalization of the one obtained in [1,2] for an infinitely long electron beam.

The first order correction to the radial force includes the effect of the electron radial motion. Inspection of the transverse phase space plots, (x', x), where

$x' = \beta_x/\beta_z$, obtained from the numerical calculations reveals that the electrons acquire a significant radial motion (see Figure 6). Let

$$B_\theta = B_\theta^0 + B_\theta^1, \tag{12}$$

where B_θ^1 is the correction term arising from a non-vanishing radial velocity of the electrons. B_θ^1 is obtained from Ampere's law

$$\nabla \times \vec{B} = \frac{4\pi}{c}\vec{J} + \frac{1}{c}\frac{\partial \vec{E}}{\partial t}, \tag{13}$$

whose projection along the radial direction is

$$\frac{\partial B_\theta}{\partial z} + \frac{1}{c}\frac{\partial E_r}{\partial t} = -\frac{4\pi}{c}J_r. \tag{14}$$

We substitute Eq. (12) into (14) and observe that the homogenous part of Eq. (14) is satisfied by B_θ^0, and the result is

$$\frac{\partial B_\theta^1}{\partial z} = -\frac{4\pi\beta}{c}J_r. \tag{15}$$

The radial momentum equation for the electrons is $\frac{\mathrm{d}}{\mathrm{d}t}(m\gamma v_r) = eE_r(1 - \beta_0)$. The numerical calculations indicate that the electron radial excursion and its energy change is quite limited in the initial phases of the pinch. Hence, the radial momentum equation can be integrated at the onset of the constriction with the assumption that γ_0 and E_r are constant along the electron trajectory. The resulting j_r is

$$j_r = -\frac{e}{\gamma_0 mc}\frac{1 - \beta_0}{\beta_0}\rho(z, r)E_r^0 z, \tag{16}$$

where the relationship $\frac{\mathrm{d}}{\mathrm{d}t} = -\beta_0 c\frac{\mathrm{d}}{\mathrm{d}z}$ has been used. We substitute Eq. (16) into (15) and integrate, and the result, at the center of the electron bunch ($\zeta = 0$), is

$$B_\theta^1 = \left(\frac{z_c}{z_s}\right)^2 E_r^0, \tag{17}$$

where, at $z_c = 0$, the electron bunch is at the beginning of the drift tube, and

$$z_s = \left(\frac{\sqrt{2\pi}I_A a^2 \sigma}{4Qc}\frac{\gamma\beta}{1 - \beta}\right)^{1/2}$$

$$\cong \left(\frac{\sqrt{2\pi}I_A a^2 \sigma}{2Qc} \gamma^3 \beta \right)^{1/2}, \tag{18}$$

where $I_A = mc^3/e$ is the Alfven current with value 1.7×10^4 [Amps], or 3.12×10^{13} [StatAmps].

We substitute Eqs. (18) and (12) into the Lorentz force and obtain the first order correction to Eq. (11), the electron radial force:

$$F_s = \left(1 - \beta^2 - \beta \left(\frac{z_c}{z_s} \right)^2 \right) E_r^0. \tag{19}$$

Eq. (19) indicates that, at sufficiently large z_c values, the radial force will be turned inward. The expression for z_s shows that high charge and low energy beams will become more constricted than their counterparts with lower charge and higher energies. For an electron bunch with Gaussian longitudinal charge density distribution, such as the one considered in this paper, E_r^0 peaks at the center of the pulse. Consequently, the maximum constriction will also occur at the center of the pulse as has been observed in the numerical calculations.

2.2 Calculation of the space charge potential

An estimate of the initial space charge potential at the beginning of the drift region has been made via the following procedure. The space charge potential Φ' is first computed in the electron rest frame $\mathbf{K}'$ which moves along z with velocity $v = \beta_0 c$ relative to the laboratory frame $\mathbf{K}$. In $\mathbf{K}'$, the electrons are stationary, the electron relative motion is neglected, the electric potential is a well-defined quantity, and it satisfies the Poisson equation. Φ' is then transformed back into the laboratory frame $\mathbf{K}$, where, from energy conservation, it is translated to an equivalent $\Delta\gamma$. The details of the procedure are as follows:

$$\Phi'(\zeta',r) = -\int_{-\infty}^{\zeta'} \mathrm{d}\eta E'_z(\eta,r) = \Phi'(\zeta,r) = -\gamma \int_{-\infty}^{\zeta} \mathrm{d}\eta E_z(\eta,r), \tag{20}$$

where $\Phi'(\zeta,r)$ transforms as the fourth component of a vector in the four-dimensional space-time space. Thus, we obtain

$$\Phi(\zeta,r) = -\gamma^2 \int_{-\infty}^{\zeta} \mathrm{d}\eta E_z(\eta,r). \tag{21}$$

6

Energy conservation gives

$$\gamma_0 mc^2 = \gamma mc^2 - e\gamma^2 \int\limits_{-\infty}^{\zeta} \mathrm{d}\eta E_z(\eta, r).$$ (22)

$E_z(\eta, r)$ is obtained from Eq. (7) (for $r < a$). Thus,

$$\Delta\gamma(\zeta, r) = \frac{2Qe\gamma_0}{mc^2 a} \int\limits_{-\infty}^{\infty} \mathrm{d}k \left(\mathrm{e}^{\mathrm{i}k\zeta} - \mathrm{e}^{-\mathrm{i}k\zeta_0}\right)/(\mathrm{i}k)$$
$$\times \left[\pi\chi(q)J_0(qr) + 2\gamma/(\mathrm{i}ak)\right],$$ (23)

where ζ_0 is arbitrary, provided it satisfies the condition $\zeta_0 >> \sigma$. Finally, we compute the normalized momentum z-component

$$\gamma\beta_z = \left[(\gamma_0 + \Delta\gamma(\zeta, r))^2 - 1\right]^{1/2}.$$ (24)

In the derivation of Eq. (24), the electrons are assumed to be strictly stationary in $\mathbf{K}'$. When significant radial motion is present, the results of this analysis will be inaccurate as is observed in the numerical results.

3 Numerical simulation results

The numerical calculations of a cylindrical, axisymmetric electron bunch in a drift tube with perfect wall conductivity were performed with the "particle in a cell" code ARGUS [5]. ARGUS is a fully three-dimensional and time-dependent (x, y, z, t) solver for Maxwell's equations. We used the "pic" solver option.

We also compared ARGUS results to the calculations from the standard code PARMELA [6]. PARMELA was originally developed at Los Alamos National Laboratory and is widely used within the accelerator community. In PARMELA, the forces between the electrons are computed in the electron rest frame where all the electron relative motion is neglected.

3.1 ARGUS results

The electron bunch is generated at $z = 0$, and the electron density conforms to Eq. (1). The total electron bunch length in our simulation is 5.0 σ's. σ varies

from 0.1274 to 0.7644 [cm]. The bunch radius a varies from 0.1 to 0.3 [cm], the electron energy E from 20. to 100. [MeV], and the charge Q from 2.0 to 18.0 [nC]. The electrons are injected with uniform β_z, and $\beta_x = \beta_y = 0$.

In the code the electrons are represented by "macro particles". The density of the macro particles is uniform, but the charge is weighted to reproduce the appropriate charge density distribution. The drift tube, as represented in ARGUS, is shown in Figure 2.
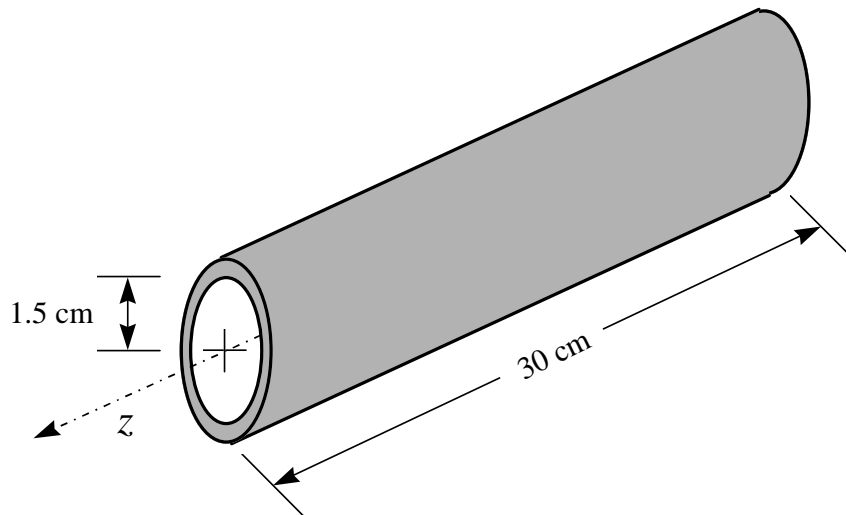

Fig. 2. Drift tube geometry in ARGUS. The positive z-axis is oriented in the direction of the bunch motion.

The drift tube radius is 1.5 [cm] and the length is 30.0 [cm]. The number of grid points along x and y is 57, and the number along z varies from 192 to 571. The spacing in x and y is not uniform: the smaller spacing (0.02 [cm]) is used in proximity of the z-axis of the tube, and the larger spacing (0.163 [cm]) in the vicinity of the wall. The spacing along z is constant. The time step, 0.35 [ps], is selected such that the Courant condition is satisfied everywhere. This condition is $v_p \Delta t \leq \Delta x_{\min}/2$, where v_p is the particle velocity, Δt is the time step, and $\Delta x_{\min}$ is the smallest grid spacing.

In Figure 3 the evolution of the (x, ζ) bunch envelope at different positions in the drift is shown. In view of the cylindrical symmetry of the electron bunch, the (x, ζ) envelope is identical to the (y, ζ) one. At $z_c = 0$. the cross section is uniform, in the interval $10. < z_c < 20.$ [cm] a small pinch develops, and at $z_c = 30.$ [cm] a fully evolved pinch has been established. The largest pinch occurs in the middle of the bunch in correspondence to the maximum radial force as also seen in Eq. (19). A close inspection of the bunch envelope reveals a tapering of the rear half. The wake fields from the front half may be responsible for this behavior.
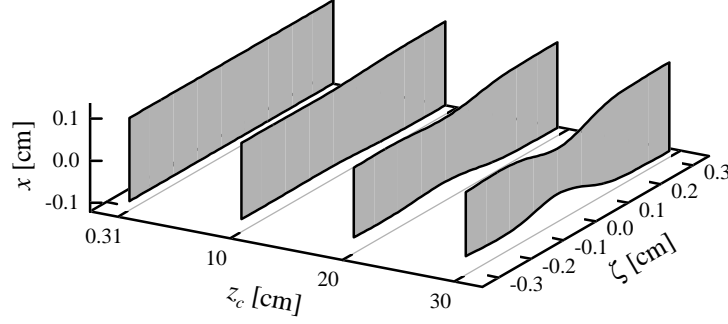
Fig. 3. Evolution of the bunch envelope. Bunch parameters: $Q = 2.0$ [nC], $a = 0.1$ [cm], $\sigma = 0.1274$ [cm], $b = 1.5$ [cm], $E = 20.$ [MeV], $\gamma_0 = 40.138$.

In Figure 4 the evolution of the longitudinal phase space, $\gamma\beta_z$ vs ζ, is presented for the same case as in Figure 3. In the inset of Figure 4(a) we have overlapped, with an expanded scale, the results of Eq. (24) with the ARGUS calculations for purpose of comparison. Here, the lower curve corresponds to $r = 0$ and the upper one to $r = a$. The agreement is quite satisfactory in view of the simplifying assumptions made in our analytical formulation. As the pulse drifts in the tube, the relative electron motion increases, and a more complex longitudinal phase space evolves.
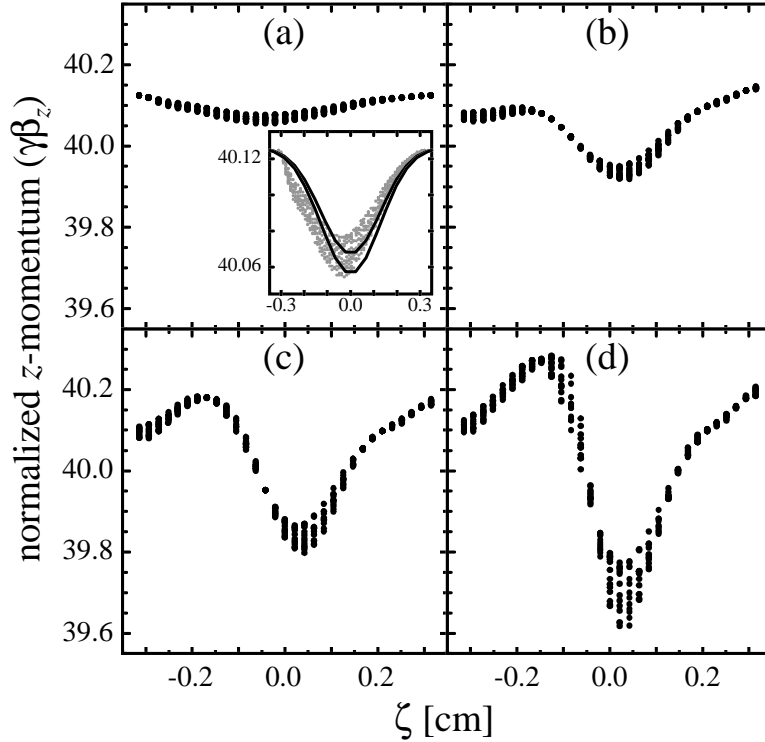
Fig. 4. Evolution of the longitudinal phase space at drift positions (a) $z_c = 0$, (b) $z_c = 10.$ [cm], (c) $z_c = 20.$ [cm], and (d) $z_c = 30.$ [cm]. Bunch parameters: $Q = 2.0$ [nC], $a = 0.1$ [cm], $\sigma = 0.1274$ [cm], $b = 1.5$ [cm], $E = 20.$ [MeV], $\gamma_0 = 40.138$.

9

In Figure 5 the phase space (x', x, z) is shown at $z_c = 0$ and $z_c = 30.$ [cm]. At $z_c = 0$ the phase space is planar as expected from the initial conditions inposed on the momemtum of the electrons. At $z_c = 30.$ [cm] the phase space has become twisted. A projection of the intersection of the phase space with the $\zeta = 0$ plane, where the largest pinch occurs, is displayed on the rear panel of the figure. A significant inward motion of the electrons is present.
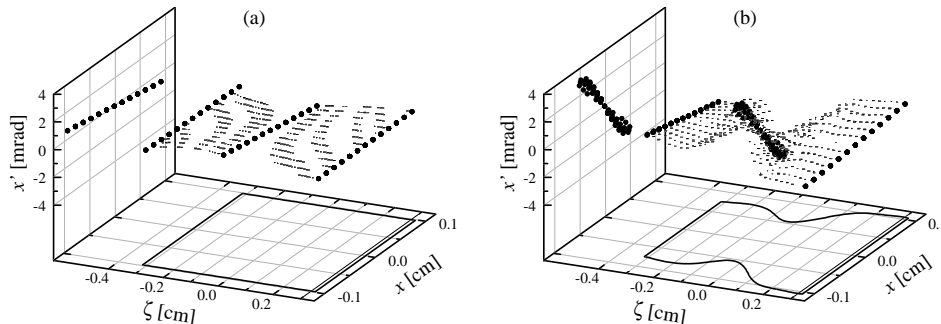

Fig. 5. Evolution of the (x', x, ζ) phase space at drift positions (a) $z_c = 0$ and (b) $z_c = 30.$ [cm]. The pulse envelope is projected on the bottom panel. Bunch parameters: $Q = 2.0$ [nC], $a = 0.1$ [cm], $\sigma = 0.1274$ [cm], $b = 1.5$ [cm], $E = 20.$ [MeV], $\gamma_0 = 40.138$.

In Figure 6 the intersections of the phase space (x', x, z) with planes at constant ζ are shown when the pulse is at the end of the drift tube, $z_c = 30.$ [cm]. Figure 6(a) and 6(b) correspond to the tail and the middle of the bunch, respectively. The entire (x', x) phase space is shown in Figure 12(a).
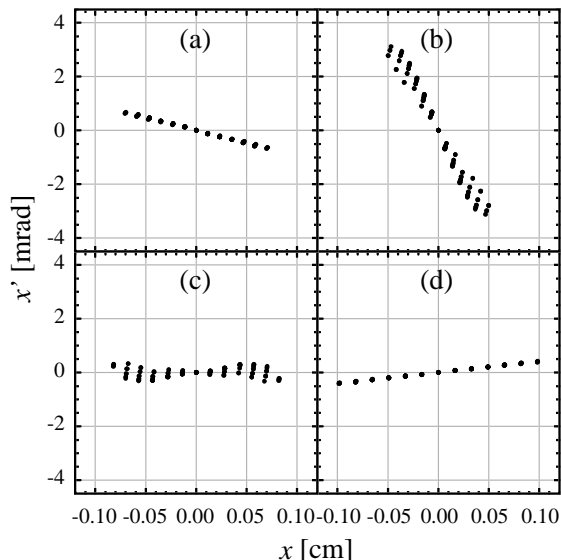

Fig. 6. Intersections of the (x', x, ζ) phase space at drift position $z_c = 30.$ [cm]. Intersections are at (a) $z = -0.315$ [cm], (b) $z = -0.030$ [cm], (c) $z = +0.094$ [cm], and (d) $z = +0.315$ [cm]. Bunch parameters: $Q = 2.0$ [nC], $a = 0.1$ [cm], $\sigma = 0.1274$ [cm], $b = 1.5$ [cm], $E = 20.$ [MeV], $\gamma_0 = 40.138$.

It is convenient to introduce the concept of the fractional rms "slice" emittance. The total normalized rms emittance of the pulse is defined as

$$\varepsilon_{\text{rms}}^{N} = \gamma\beta \left[\pi \left(\left\langle x^2 \right\rangle \left\langle x'^2 \right\rangle - \left\langle xx' \right\rangle^2 \right)^{1/2} \right], \qquad (25)$$

where the averages indicated by the angle brackets, $\langle\rangle$, extend over all the pulse particles. The fractional slice emittance is defined as

$$\varepsilon_{\text{rms},f}^{N}(\zeta, \Delta\zeta) = \gamma\beta \left[\pi \left(\left\langle x^2 \right\rangle_{\Delta\zeta} \left\langle x'^2 \right\rangle_{\Delta\zeta} - \left\langle xx' \right\rangle_{\Delta\zeta}^2 \right)^{1/2} \right] / \varepsilon_{\text{erms}}^{N}, \qquad (26)$$

where the averages indicated by the angle brackets, $\langle\rangle_{\Delta\zeta}$, are limited to particles within the slice, i.e. with ζ-coordinate between ζ and $\zeta + \Delta\zeta$.

In Figure 7(a) the pulse current profile at $z_c = 0$ and $z_c = 30.$ [cm] is shown. The current profiles are nearly identical, as expected, because of the limited relative longitudinal motion among the particles. In Figure 7(b) the fractional slice emittance as a function of ζ for different position z_c along the drift tube is shown. Observe that the fractional slice emittance is always significantly smaller than the total pulse emittance of 18.5 [π mm-mrad] at the end of the drift tube. This indicates that the pulse emittance is strongly correlated.
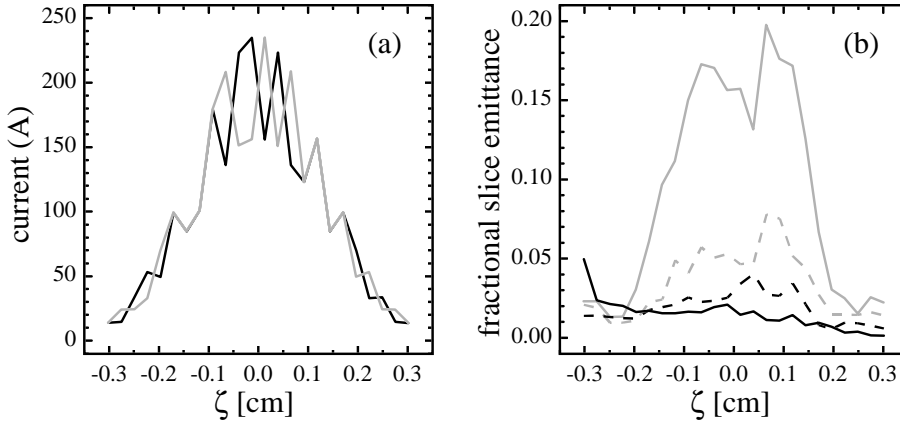

Fig. 7. (a) Bunch current and (b) fractional slice emittance vs position in the bunch at different locations in the drift tube. All fractional slice emittances in (b) are normalized to 18.5 [π mm-mrad]. Legend: dark solid line, $z_c = 0.66$ [cm]; dark broken line, $z_c = 10.$ [cm]; light broken line, $z_c = 20.$ [cm]; light solid line, $zc = 30.$ [cm]. Bunch parameters: $Q = 2.0$ [nC], $a = 0.1$ [cm], $\sigma = 0.1274$ [cm], $b = 1.5$ [cm], $E = 20.$ [MeV], $\gamma_0 = 40.138$. Curve fluctuations are due to discretization noise.

In Figure 8 typical longitudinal (ζ, x) bunch envelopes at $zc = 30.$ [cm] are presented, corresponding to varying energies, bunch lengths, and charges. The pinch decreases at higher energies and increases with bunch length for constant charge density.
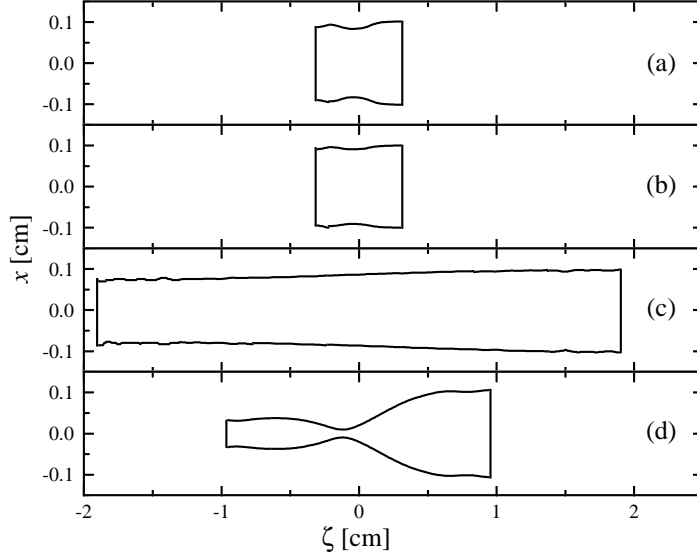
Fig. 8. Various longitudinal (ζ, x) bunch envelopes at drift location $z_c = 30.$ [cm].
For (a)–(d), $a = 0.1$ [cm]. Bunch parameters:
(a) $Q = 2.0$ [nC], $\sigma = 0.1274$ [cm], $b = 0.25$ [cm], $E = 50.$ [MeV], $\gamma_0 = 98.84$
(b) $Q = 2.0$ [nC], $\sigma = 0.1274$ [cm], $b = 0.25$ [cm], $E = 100.$ [MeV], $\gamma_0 = 196.69$
(c) $Q = 2.0$ [nC], $\sigma = 0.7639$ [cm], $b = 0.25$ [cm], $E = 20.$ [MeV], $\gamma_0 = 40.13$
(d) $Q = 6.0$ [nC], $\sigma = 0.3822$ [cm], $b = 1.5$ [cm], $E = 20.$ [MeV], $\gamma_0 = 40.13$.

The evolution of the pinch ratio as a function of the position in the drift tube is
shown in Figure 9(a). Here, $r_{\min}/a$, the ratio of the minimum bunch envelope
radius divided by the initial bunch radius, is plotted versus the position in the
drift tube for three different values of the bunch energy. Higher energy bunches
undergo less pinching than lower energy ones. In Figure 9(b), $r_{\min}/a$ is plotted
versus the normalized bunch center position, z_c/z_s. The three separate curves
of Figure 9(a) nearly collapse into a single one, thus showing that Eq. (18)
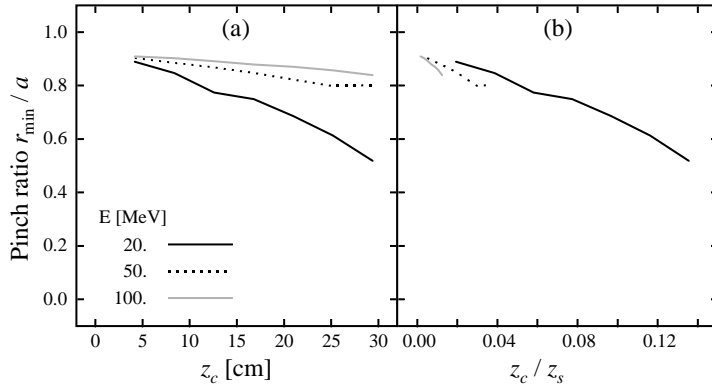correctly captures the energy scaling of the pinch ratio.

Fig. 9. Pinch ratio vs (a) drift position z_c and (b) normalized drift position z_c/z_s
in the drift tube for various initial energies. Common bunch parameters: $Q = 2.0$
[nC], $a = 0.1$ [cm], $\sigma = 0.1274$ [cm], $b = 0.25$ [cm].

12

In Figure 10 the evolution of the pinch ratio is shown as a function of z_c/z_s for pulses of different diameters, same lengths and different charges selected to maintain a constant electron density. As in the previous case, the pinch ratio is well parameterized by z_c/z_s.
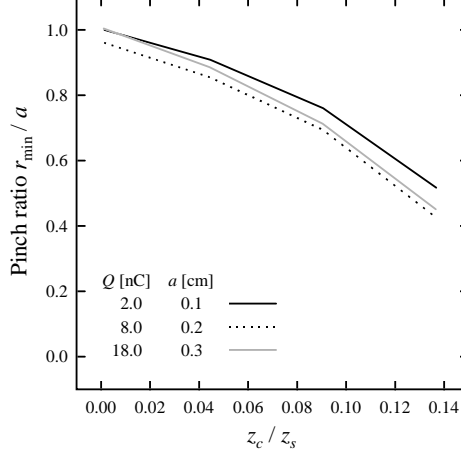

Fig. 10. Pinch ratio vs normalized drift position zc/zs in the drift tube for various charges and initial bunch radii. Common bunch parameters: $\sigma = 0.1274$ [cm], $b = 1.5$ [cm], $E = 20.$ [MeV], $\gamma_0 = 40.138$.

Finally, in Figure 11 the evolution of the pinch ratio is shown as a function of z_c/z_s for bunches of different lengths, identical transverse cross sections and different charges selected to maintain a constant electron density. Unlike the previous cases, the pinch ratio is not well parameterized by z_c/z_s. The probable explanation for the inability to parameterize the present case is that the wake fields of the particles in the leading edge of the bunch are not properly accounted for in our simple theory.
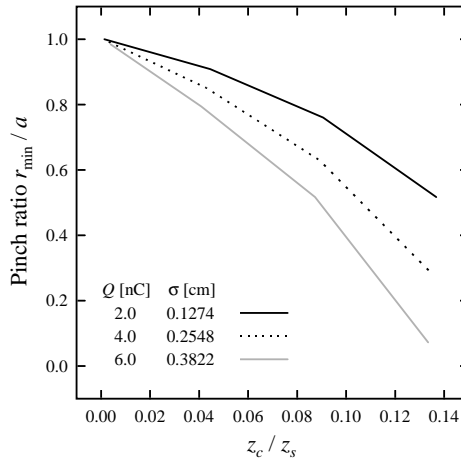

Fig. 11. Pinch ratio vs position z_c/z_s in the drift tube for various charges and bunch lengths. Common bunch parameters: $a = 0.1$ [cm], $b = 1.5$ [cm], $E = 20.$ [MeV], $\gamma_0 = 40.138$.

13

ARGUS and PARMELA yield quite different results for identical bunch conditions. In Figure 12 the transverse phase space, as computed by ARGUS and PARMELA at $z_c = 30.$ [cm], is shown. The PARMELA phase space reflects only a mild defocusing effect due to the space charge. The ARGUS counterpart combines the focusing and defocusing due to the pinching force.
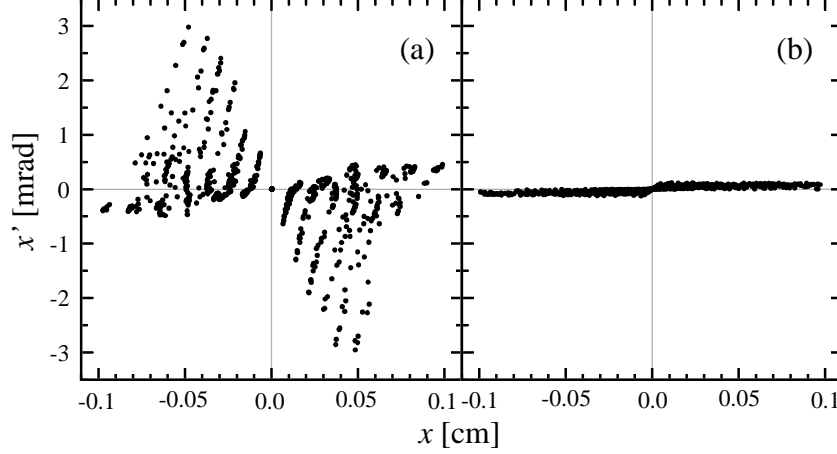

Fig. 12. (a) ARGUS and (b) PARMELA results of transverse (x, x') phase space at drift position $z_c = 30.$ [cm]. Bunch parameters: $Q = 2.0$ [nC], $a = 0.1$ [cm], $\sigma = 0.1274$ [cm], $b = 1.5$ [cm], $E = 20.$ [MeV], $\gamma_0 = 40.138$.

In Figure 13 the longitudinal phase space, as computed by ARGUS and PARMELA at $z_c = 30.$ [cm], is shown. Here, PARMELA cannot reproduce the complexity of the longitudinal momentum distribution within the bunch.
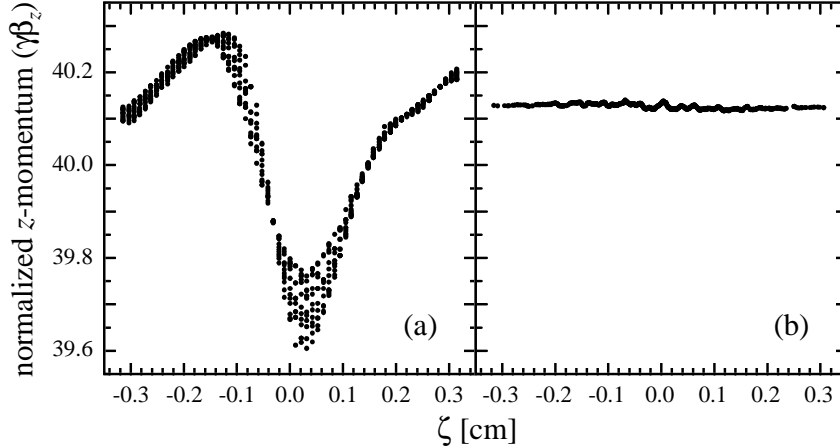

Fig. 13. (a) ARGUS and (b) PARMELA results of longitudinal $(\gamma\beta_z, \zeta)$ phase space at drift position $z_c = 30.$ [cm]. Bunch parameters: $Q = 2.0$ [nC], $a = 0.1$ [cm], $\sigma = 0.1274$ [cm], $b = 1.5$ [cm], $E = 20.$ [MeV], $\gamma_0 = 40.138$.

Finally, in Figure 14 the longitudinal (ζ, x) envelopes at $z_c = 30.$ [cm], as computed by ARGUS and PARMELA, are presented. No pinching of the bunch is exhibited by the PARMELA calculations.
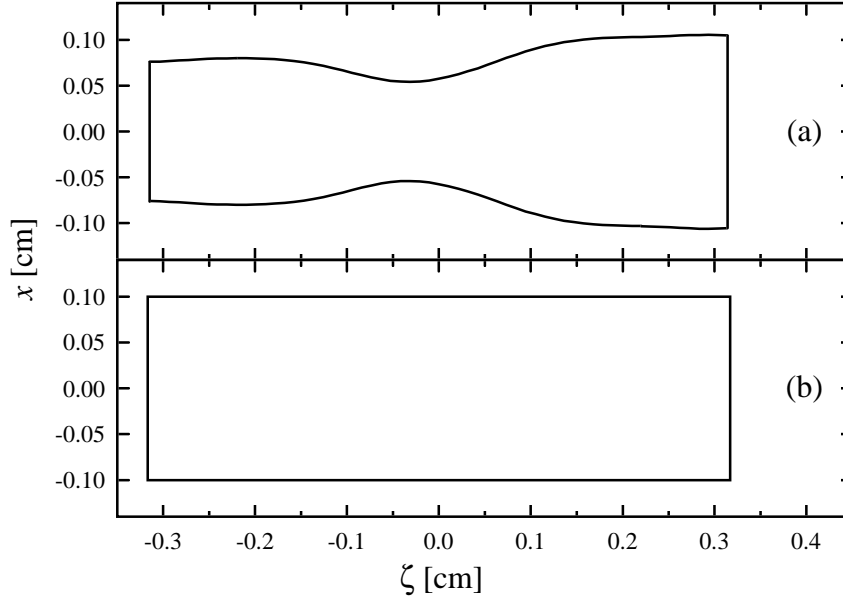

Fig. 14. (a) ARGUS and (b) PARMELA results of longitudinal (ζ, x) bunch envelopes at drfit position $z_c = 30.$ [cm]. Bunch parameters: $Q = 2.0$ [nC], $a = 0.1$ [cm], $\sigma = 0.1274$ [cm], $b = 1.5$ [cm], $E = 20.$ [MeV], $\gamma_0 = 40.138$.

4 Summary and Conclusions

We have presented the results of extensive numerical simulations of electron bunches with charge densities ρ of the order of 10^2 to 10^3 [nC/cm³] and energies between 20. and 100. [MeV]. The results indicate the presence of a strong pinch in the middle of an electron bunch with a Gaussian longitudinal electron density distribution. The pinching force scales approximately as $\gamma^{-3/2}$ and $r^{1/2}$. This force generates an increase in the correlated bunch emittance, and the space charge depression is also affected. A simplified analysis to explain these results has been described. The results are in significant disagreement with the ones obtained from the standard accelerator code PARMELA. This is attributed to the neglect of the electron relative motion in the space charge calculations performed in PARMELA.

The pinch effects we have uncovered will play a significant role in the photoinjectors used in Free Electron Laser and other high-brightness accelerators. Here, the electron pulse has very low energy, and this will limit the allowed charge density in order to avoid undue pinching and space charge effects. The break up of the electron bunch at the photoinjector has been observed [7,8]

and attributed solely to the longitudinal component of the space charge force. The pinching force discussed in this paper may also play a role. In addition, the design of magnetic pulse compressors will need to account for the pinch which may become significant in the last stage of the compression.

Further analytical studies and numerical simulations are necessary to better understand (a) the evolution of the pinch as $z_c \to \infty$ and (b) the effect of the longitudinal electron density distributions. Preliminary indications are that uniform longitudinal charge density distributions become pinched at multiple positions in the bunch. The pinch period depends upon the pulse parameters. More importantly, experimental observation of the pinch is needed to completely validate these results.

Acknowledgements

References

[1] A. Woo Tao, *Physics of Collective Beam Instabilities in High Energy Accelerators* (John Whiley & Sons, New York, 1993).

[2] M. Reassure, *Theory and Design of Charged Particle Beams* (John Wiley & Sons, New York, 1994).

[3] P. L. Morton, V. K. Neil, A. M. Sessler, *Jour. App. Phys.* **37** (1966) 3875.

[4] *Handbook of Mathematical Functions*, M. Abramowitz, I. A. Stegun, eds., (Dover Publications, Inc., 1974).

[5] ARGUS is a commercial product developed by Science Application International Corporation (SAIC™).

[6] P. Zhou, R. G. Carter, *A User's Guide to PARMELA*, Report MRG/89/3 (Lancaster University, May 1989).

[7] A. Loulergue, D. H. Dowell, S. Joly, J. P. de Brion, G. Haouat, F. Schumann, *Nuc. Instr. & Meth. in Phys. Res.* **384** (1997) 285-292.

[8] D. H. Dowell, S. Joly, J. P. de Brion, G. Haouat, A. Loulergue, *Proceedings of the Seventeenth International Free Electron Laser Conference*, I. Ben-Zvi and S. Krinsky, eds. (North-Holland, Amsterdam, 1996) 104-107.